

Chromatic and spatial properties of parvocellular cells in the lateral geniculate nucleus of the marmoset (*Callithrix jacchus*)

Esther M. Blessing^{1,2,3}, Samuel G. Solomon³, Maziar Hashemi-Nezhad⁴, Brian J. Morris³ and Paul R. Martin^{1,2,3}

¹National Vision Research Institute of Australia, Cnr Keppel and Cardigan Streets, Carlton, VIC 3053, Australia

²Department of Optometry and Vision Sciences, The University of Melbourne, Parkville, VIC 3052, Australia

³Discipline of Physiology, the University of Sydney, New South Wales 2006, Australia

⁴Discipline of Anatomy and Histology, the University of Sydney, New South Wales 2006, Australia

The parvocellular (PC) division of the afferent visual pathway is considered to carry neuronal signals which underlie the red–green dimension of colour vision as well as high-resolution spatial vision. In order to understand the origin of these signals, and the way in which they are combined, the responses of PC cells in dichromatic (‘red–green colour-blind’) and trichromatic marmosets were compared. Visual stimuli included coloured and achromatic gratings, and spatially uniform red and green lights presented at varying temporal phases and frequencies.

The sensitivity of PC cells to red–green chromatic modulation was found to depend primarily on the spectral separation between the medium- and long-wavelength-sensitive cone pigments (20 or 7 nm) in the two trichromatic marmoset phenotypes studied. The temporal frequency dependence of chromatic sensitivity was consistent with centre–surround interactions. Some evidence for chromatic selectivity was seen in peripheral PC cells. The receptive field dimensions of parvocellular cells were similar in dichromatic and trichromatic animals, but the achromatic contrast sensitivity of cells was slightly higher (by about 30%) in dichromats than in trichromats. These data support the hypothesis that the primary role of the PC is to transmit high-acuity spatial signals, with red–green opponent signals appearing as an additional response dimension in trichromatic animals.

(Received 13 November 2003; accepted after revision 24 March 2004; first published online 26 March 2004)

Corresponding author P. R. Martin: National Vision Research Institute of Australia, Cnr Keppel and Cardigan Streets, Carlton, VIC 3053, Australia. Email: prmartin@unimelb.edu.au

This study concerns the functional specialization of sub-cortical visual pathways for colour and spatial vision. Early electrophysiological studies in the primate retina and the dorsal lateral geniculate nucleus (LGN) revealed the existence of visually responsive neurones which showed antagonistic interaction between signals originating in the distinct (‘red’ or L; ‘green’ or M; and ‘blue’ or S) spectral classes of cone photoreceptor (De Valois *et al.* 1966; Wiesel & Hubel, 1966). A subset of these cone-opponent cells – mostly those receiving input from S cones – showed little evidence of spatial antagonism, consistent with functional specialization for transmitting chromatic signals (Wiesel & Hubel, 1966). Subsequent studies showed that the majority of neurones in the parvocellular (PC) layers of the LGN display at least some degree of opponency between M and L cones (De Monasterio *et al.* 1975; Derrington *et al.*

1984; Lee *et al.* 1987), showing that the PC pathway could transmit neuronal signals that serve the red–green dimension of colour vision. However, most PC cells also have relatively small, spatially antagonistic receptive fields, consistent with functional specialization for high-acuity spatial vision. The question of whether the PC pathway is specialized to serve one or other of these submodalities of vision is a matter of controversy (Ingling & Martinez, 1985; Shapley & Perry, 1986; Rodieck, 1991; Reid & Shapley, 2002).

On the one hand, the poor contrast sensitivity of PC cells and relatively poor temporal precision of PC cell responses suggest that this pathway is specialized to transmit ML opponent signals at the expense of spatial precision (Crook *et al.* 1988; Lee *et al.* 1993; Reid & Shapley, 2002). On the other hand, the spatial opponency and small receptive field

size (when measured with high-contrast stimuli), and the high sampling density of the PC cell array are consistent with the idea that a primary role of the PC pathway is to serve high-acuity spatial vision (Dreher *et al.* 1976; Derrington & Lennie, 1984; Lennie *et al.* 1991; Wässle & Boycott, 1991). In this view, the ML opponent signal is generated as a 'by-product' of retinal circuitry for high spatial resolution vision (Paulus & Kröger-Paulus, 1983; Mollon & Jordan, 1988; Lennie *et al.* 1991).

If the PC cells are specialized for high-acuity spatial vision, then changes in the complement and spectral position of M and L cones should alter the sensitivity to chromatic variation without compromising other aspects of PC cell performance such as achromatic contrast sensitivity and spatial resolution. Here, we test this hypothesis in experimental studies of a primate species that shows polymorphic colour vision.

In common with many other species of New World monkeys (Mollon *et al.* 1984; Jacobs, 1996) the marmoset *Callithrix jacchus* shows a sex-linked polymorphism of red–green colour vision. A single gene on the X chromosome encodes for one of three alleles of ML-cone pigments. The pigments have maximal sensitivity close to 543 nm, 556 nm and 563 nm (Travis *et al.* 1988; Tovée *et al.* 1992). Yeh *et al.* (1995) studied a family of marmosets carrying the 543 nm and 563 nm alleles, and showed that many PC cells in trichromatic females showed red–green opponent responses. Lee *et al.* (2000) measured temporal response properties of PC pathway ganglion cells in another New World species, the capuchin monkey *Cebus apella*. They found little difference in temporal properties between dichromatic and trichromatic animals. These studies and subsequent studies in marmosets (Kremers *et al.* 1997; Weiss *et al.* 1998; White *et al.* 1998; Kilavik *et al.* 2003) showed that there is a temporal delay in the inhibitory opponent input to PC cells. Thus, as in macaque (Gouras & Zrenner, 1979; Smith *et al.* 1992), the red–green opponent responses in New World monkeys could arise from centre–surround interactions in the receptive field.

In the present study, we compared PC cell responses to chromatic and spatial variation in two trichromatic phenotypes, and three dichromatic phenotypes, in marmosets. We measured responses to both achromatic spatial contrast and temporal-chromatic contrast in the same cells, allowing correlation between these properties to be made. The results are consistent with the hypothesis that the responses of PC cells are governed by requirements for transmission of high-acuity spatial signals, and that the ML opponent signal in trichromatic marmosets is a subsidiary property of receptive fields designed for high spatial acuity.

Methods

Genotyping

Genomic DNA was extracted from whole blood samples using the QIAamp blood extraction kit (QIAGEN, Hilben, Germany). Exons 2 and 5 of the marmoset X-linked opsin gene were amplified by polymerase chain reaction (PCR). Primer pairs for amplification of each exon were designed from the sequences published by Hunt *et al.* (1993). The sequences for exon 2 primers were as follows: forward: 5'-CTT CGA AGG CCC CAA TTA-3', reverse: 5'-ACA GGG AGA CGG TGT AGC-3', and for exon 5: forward: 5'-GAA TCT ACC CAG AAG GCA GA-3', reverse, 5'-ATG GGG TTG TAG ATA GTG GC-3'. The PCR mixture was 150 nmol of genomic DNA; 260 μ mol l⁻¹ each dNTP, 40 nmol l⁻¹ each primer, 2 nmol l⁻¹ MgCl₂, 50 nmol l⁻¹ KCl, 10 mmol l⁻¹ Tris HCl at pH 8.3, and 0.1 U AmpliTaq Gold (Applied Biosystems, CA, USA). The following hot-start protocol was used: 94°C for 2 min; 35 cycles at 94°C for 1 min, 65°C for 40 s, and 72°C for 1 min. These cycles were followed by a step at 72°C for 10 min. Reaction mixtures were then cooled to 4°C. The PCR products for exons 2 and 5 were 290 and 215 bp in length, respectively. The restriction endonucleases *Bgl*II (Promega, Sydney), *Hpy*CH4III (New England Biolabs, USA) and *Pvu*I (Promega, Sydney) were used to identify the 543 nm (*P543*), 556 nm (*P556*), and 563 nm (*P563*) alleles of the marmoset X-linked opsin gene polymorphisms. The criterion sizes (bp) of restriction fragments generated by cleavage at each restriction site were: *Bgl*II, 235, 55, *Hpy*CH4III, 150, 65, *Pvu*I, 170, 120. Example RFLP-PCR results are shown in Fig. 1.

Animal preparation and recording

Recordings were made from 16 adult marmosets (*Callithrix jacchus*) of body weight 280–380 g. The genotype of 15 of these animals was established prior to the electrophysiological experiments. Animals were obtained from the Australian National Health and Medical Research Council (NHMRC) combined breeding facility. Nine of the animals were female. All procedures used conform to the provisions of the NHMRC code of practice for the care and use of animals. All animals were initially anaesthetized with isoflurane (Forthane, Abbott, Sydney, 1.5–2%) and intramuscular ketamine (Ketalar, Parke-Davis, Sydney, 30 mg kg⁻¹) for surgery. A femoral vein and the trachea were cannulated. Animals were artificially respired with a 70% : 30% mixture of NO₂ : carbogen (5% CO₂ in O₂). A venous infusion of 40 μ g kg⁻¹ alcuronium chloride (Alloferin, Roche, Sydney) in dextrose Ringer

solution (Baxter, Sydney, Australia) was infused at a rate of 1 ml h^{-1} to maintain muscular relaxation. Anaesthesia was maintained during recording with a venous infusion of sufentanil citrate (Sufenta-Forte, Janssen-Cilag, Beerse, Belgium; $4\text{--}8 \mu\text{g kg}^{-1} \text{ h}^{-1}$). Electroencephalogram (EEG) and electrocardiogram signals were monitored to ensure adequate depth of anaesthesia. Criteria for adequate analgesia were almost complete dominance of low-frequency ($<8 \text{ Hz}$) components of the EEG and stability of both the EEG signal and heart rate under intermittently applied noxious stimuli such as tail or paw-pinch. End-tidal CO_2 was maintained near 4% by adjusting the rate and depth of ventilation, and body temperature was kept near 37.5°C . Pupils were dilated with topical neosynephrine (Sterling-Winthrop, New York). Penicillin (Aquacaine, CSL Australia, Melbourne, Australia) and corticosteroids (Decadron, Merke, Sharpe & Dohme, Sydney, Australia) were administered daily. The typical duration of a recording session was 72 h.

The animal was mounted in a stereotaxic head-holder. The eyes were protected by oxygen-permeable contact lenses and focused on a tangent screen 114 cm from the animal. The positions of the fovea and optic disc were mapped with the aid of a fundus camera. A craniotomy was made over the LGN and a microelectrode (parylene-coated tungsten or glass-coated steel; impedance 5–12 $\text{M}\Omega$, F.H. Haere Co., Bowdoinham, ME, USA) was lowered into the LGN. Action potentials arising from visually responsive cells were identified and the time of their occurrence measured to an accuracy of 0.1 ms. Responses were subjected to Fourier analysis; the first harmonic amplitude and phase were used as response measures.

Visual stimuli

Each visually responsive cell was initially classified using hand-held stimuli and its receptive field mapped on the tangent screen. A front-silvered gimbal mirror was then placed in the optical path, and its angle adjusted to position the receptive field of the cell at the centre of a CRT monitor. The optical path length was 114 cm. Visual stimuli were generated using a VSG Series Three video signal generator (Cambridge Research Systems, Cambridge, UK) and presented on a Reference Calibrator Plus (Barco) monitor at a frame refresh rate of 100 Hz. The video signal generator incorporates a photometric feedback system for colorimetric specification and gamma correction to allow direct specification of stimuli in Commission Internationale de l'Eclairage (CIE; x , y , Y) coordinates. The accuracy of this system was verified with a PR-650 photometer (Photo Research, Palo Alto, CA, USA).

For each cell, the optimal spatial frequency, temporal frequency, orientation and contrast was determined, using achromatic drifting gratings presented within a 2 deg diameter aperture at a mean luminance of 55 cd m^{-2} . An aperture-tuning curve was measured using the optimum stimulus parameters. An aperture diameter which was slightly above the optimal diameter, and which also was an integer multiple of the optimum spatial period, was used thereafter. The reader should note that such apertures encompass both centre and surround components of the classical receptive field of PC cells (Solomon *et al.* 2002). Receptive field dimensions were estimated by difference-of-gaussians (DOG) fit to the spatial-frequency tuning curve using standard methods (White *et al.* 2001). At the low temporal frequencies used for these measurements, the phase error introduced by using the DOG fit rather than a vector model (Frishman *et al.* 1987) is very small ($<15 \text{ deg}$).

Characterization of chromatic phenotype

Responses to chromatic-spatial variation were measured using drifting sinusoidal gratings that were modulated in 144 or 62 directions about a white point (CIE D65). Grating vectors were uniformly spaced excursions in

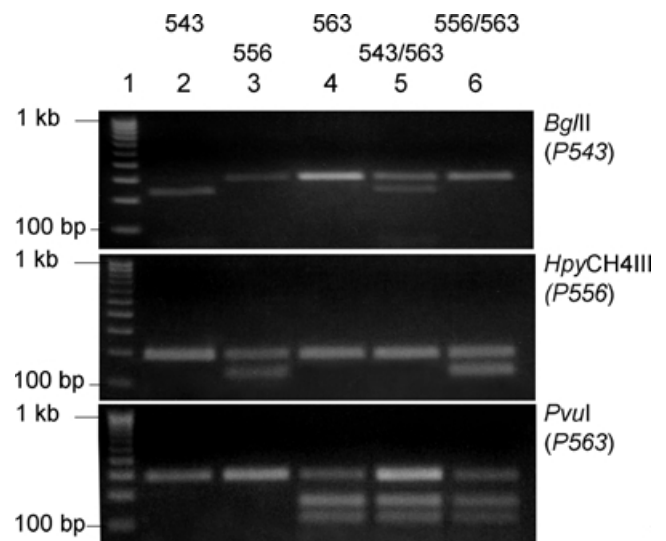


Figure 1. Identification of cone opsin-encoding genes in marmosets

Each panel shows agarose gel electrophoresis of *BglIII*, *HpyCH4III*, or *PvuI* restriction digestion products. Lane 1, molecular weight markers. Lanes 2–6, DNA amplification products from five animals: MY76, MY83, MY82, MY84 and MY85. Five of the possible genotypes predicted by the single locus model are present. The predicted phenotype is indicated by the nominal peak wavelength values above each lane.

chromaticity (CIE x, y) and luminance (CIE Y). Figure 2A shows the CIE (x, y) coordinates of the set of gratings in the isoluminant plane. The excursion vector was 'tilted' above or below this plane to measure the response to other combinations of luminance and chromatic contrast (Fig. 2B). We refer to this stimulus set as the CIE set. Coordinates in the CIE set are expressed as azimuth (relative to the CIE x dimension) and elevation (relative to CIE Y -dimension). The reader should note that the stimuli and the coordinate system were not designed to probe special directions of the colour space(s) defined by marmoset cone mechanisms. Rather, we sought a uniform set of stimuli where cell behaviour can be compared with predictions based on cone mechanisms in six different spectral phenotypes. The mean luminance was 32 cd m^{-2} . The maximum achromatic Michelson contrast was 48%. Gratings were presented at optimum temporal frequency, in two epochs of 4–7 s. The second presentation was identical to the first but had the opposite spatial phase. For computational convenience, the azimuth was assigned to be negative for this 'hemisphere' of the stimulus space.

Chromatic and temporal sensitivity measurement

Responses to chromatic-temporal variation were measured for stimuli delivered via a Maxwellian view system described in full elsewhere (Smith *et al.* 1992). Briefly, the stimulus was a spatially uniform field comprising the images of two light-emitting diodes (LEDs), with dominant wavelengths of 554 and 639 nm. For the red and green diodes together, illuminance was close to 2000 photopic trolands. Unless otherwise specified, the relative radiance of the red and green LEDs was set for equal luminance (V_λ) using a calibrated photocell.

For temporal-frequency analysis of cone inputs, the phase of the green diode was varied relative to that of the red (Smith *et al.* 1992; Yeh *et al.* 1995). Diode modulation depth was 100%. Responses were measured to 16 relative phases in steps of 22.5 deg at temporal frequencies between 1 and 30 Hz.

Contrast–response functions were measured for uniformly spaced contrast steps (2 presentations of 4–8 s duration) or by continuous contrast variation at

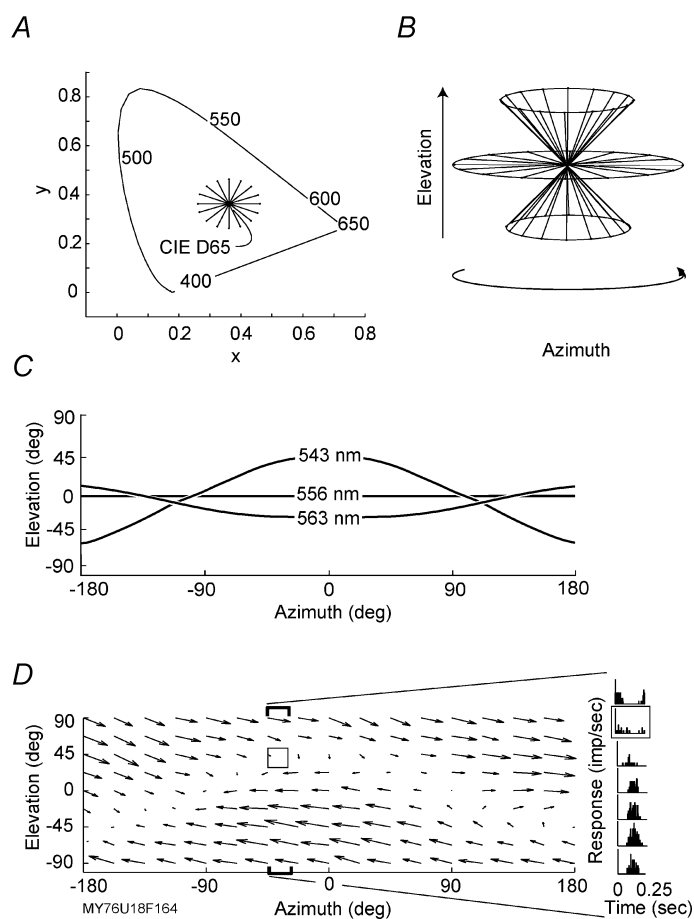


Figure 2. Analysis of spectral inputs to marmoset PC cells

The chromaticity coordinates and modulation direction of eight gratings in the isoluminant plane are indicated in A. Each modulation line bisects the central white point (CIE D65). Combined luminance and chromatic modulation was achieved by 'tilting' the modulation direction out of the isoluminant plane, as indicated in B. Each stimulus point is defined by its azimuth (relative to the CIE x -axis) and elevation (relative to the isoluminant plane). The isolept or silent substitution lines for cone fundamentals with maximum sensitivities at 543, 556 or 563 nm are shown in C. Responses of one magnocellular cell in a marmoset with the *P543* genotype are shown in D. Each arrow shows the phase and amplitude of the fundamental Fourier component (F1) of the cell response to grating modulation at the stimulus position defined by the tail of the arrow. Peri-stimulus time histograms for different elevation values at the indicated azimuth are shown to the right of the vector map (from top): 90 deg, 45 deg, 22.5 deg, 0 deg, -22.5 deg, -45 deg, -90 deg. The trajectory of the response minima can be seen to match the isolept for the 543 cone mechanism.

a carrier temporal frequency of 3.906 Hz in a sine envelope over a 4.096 s stimulus epoch (White *et al.* 1998; Solomon *et al.* 1999). The LEDs were modulated either in-phase, producing a homochromatic field that varied only in luminance, or in counter-phase, producing a heterochromatic stimulus. We refer to these paradigms as 'luminance' and 'chromatic' modulation hereinafter. The reader should note, however, that these terms are specified photometrically, and do not account for differences between the luminous efficiency function of the marmoset and human eye.

Histological processing

The position of each recorded cell was noted by reading the depth from the hydraulic microelectrode advance (David Kopf Model 640). Electrolytic lesions (6–10 $\mu\text{A} \times 6$ –10 s, electrode negative) were made to mark selected recording positions. At the conclusion of the recording session the animal was killed with an overdose of pentobarbitone sodium (80–150 mg kg⁻¹, i.v.) and the position of recorded cells in the LGN was reconstructed using standard histological methods as described fully elsewhere (Solomon *et al.* 1999; White *et al.* 2001).

Results

Genotyping

A total of 42 marmosets were genotyped by three-way RFLP-PCR. Table 1 shows the genotype of the animals from which electrophysiological data were obtained. At least one replicate experiment was carried out for the majority (29/45) of the entries shown in Table 1. All six of the possible X-linked opsin genotypes were identified in the marmoset population studied. The *P543*, *P556*, and *P563* alleles were encountered at frequencies of 42, 13 and 45%, respectively. Results for all animals were consistent with the tri-allelic single-locus X-chromosome model: all males possessed only one allele, and all females possessed either one or two alleles (Mollon *et al.* 1984; Travis *et al.* 1988; Tovée *et al.* 1992; Hunt *et al.* 1993).

Physiological confirmation of the genetic analysis

Responses of both magnocellular (MC) and parvocellular (PC) cells were analysed. Figure 2C shows the *isolept* (Rushton *et al.* 1973) or *silent substitution* (Cavonius & Estévez, 1975) loci in the CIE set for cone mechanisms with peak sensitivities at 543, 556 and 563 nm. The responses of one MC cell are shown in Fig. 2D. The response

Table 1. Analysis of cone opsin encoding genes

Colony ID	Exp	Gender	<i>Bgl</i> III	<i>Hpy</i> CH4III	<i>Pvu</i> I
m707	MY73	M	+	–	–
m779	MY79	M	+	–	–
m901	MY77	M	+	–	–
m902	MY76	M	+	–	–
m767	MY74	M	–	+	–
m695	MY82	M	–	–	+
m749	MY75	M	–	–	+
f724	MY71	F	+	–	–
f842	MY83	F	–	+	–
f693	MY90	F	–	+	+
f845	MY85	F	–	+	+
f702	MY69	F	+	–	+
f619	MY72	F	+	–	+
f847	MY89	F	+	–	+
f852	MY84	F	+	–	+

Results of three-way restriction fragment-length polymorphism-polymerase chain reaction (RFLP-PCR) are shown for three endonucleases for each animal tested. Endonucleases *Bgl*III, *Hpy*CH4III, and *Pvu*I target the 543, 556 and 563 nm alleles, respectively. Abbreviations: Colony ID, marmoset colony identification number; Exp, electrophysiology experiment identification number; M, male; F, female; +, digestion by endonuclease (indicating presence of the target allele); –, no digestion by endonuclease.

minima correspond to the isolept of the genetically predicted cone type (543 nm). We quantified the relationship between the predicted cone type and the responses of 20 PC cells and 14 MC cells in seven animals (3 female, 4 male) as follows. A set of spectral absorbance templates (nomograms) ranging in peak wavelengths between 500 and 600 nm at 1 nm intervals was generated using the polynomial templates of Baylor *et al.* (1987) or Lamb (1995). The cone contrast for each grating in the CIE set was calculated for each nomogram by convolution with the $[x, y, Y]$ coordinates of the grating components *via* the Judd-Voss modified CIE 1931 colour matching functions (Brainard, 1996). Lens absorbance was corrected using published measurements for marmoset (Tovée *et al.* 1992). The neuronal response amplitude and phase for each grating was fitted to the predicted cone contrast by minimizing the mean square error (MSE) between the data and the model using a Levenberg-Marquardt optimization routine (Matlab optimization toolbox, MathWorks Inc. Natick, MA, USA). The relative weight of phase and amplitude errors was normally adjusted so that 1 impulse s⁻¹ was equivalent to 5–10 deg phase error. This ratio gave the most efficient and reliable convergence for the great majority of stimulus conditions. In a small number of cases where

response amplitude was low, greater weight was given to the phase error to allow the fit to converge.

In agreement with previous analyses (Yeh *et al.* 1995; Weiss *et al.* 1998), the responses of PC and MC cells in dichromatic animals were well accounted for by a single cone mechanism. The residual error returned by the fitting routine is shown as a function of Baylor nomogram peak wavelength in Fig. 3A. Results from one MC pathway cell in each of the dichromat genotypes are shown. The spectral peak of the nomogram which best

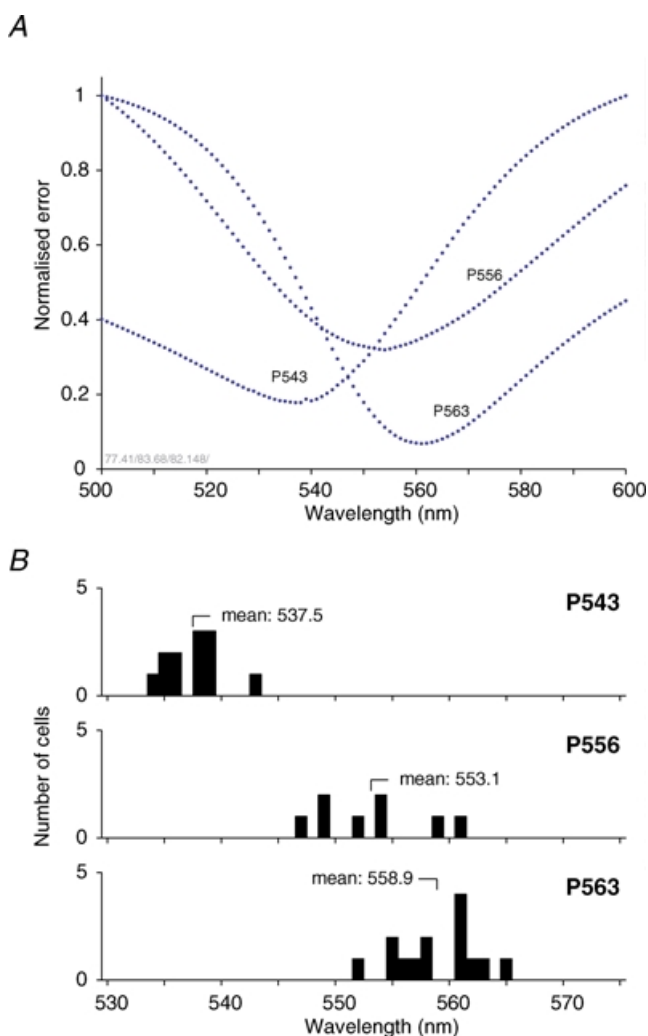


Figure 3. Correlation of phenotype with genotype in marmosets

A shows residual error from predictions of cell response amplitude as a function of peak sensitivity of cone fundamentals. Data from one magnocellular pathway cell for each dichromatic genotype are shown. The best-fitting wavelengths for these cells are: P543, 538 nm; P556, 554 nm; P563, 561 nm. Histograms in B show best-fitting wavelength for MC and PC cells recorded in animals of each tested genotype. Values for dichromatic cells are clustered close to the predicted spectral peak.

accounts for response amplitude is close to the value determined by microspectrophotometric measurements (Travis *et al.* 1988; Tovée *et al.* 1992) for the genetically predicted phenotype. Pooled data from the three dichromatic genotypes are shown as histograms in Fig. 3B. Each point on the histogram shows the spectral peak of the best-fitting nomogram for a single cell. Peak wavelength estimates obtained using the Baylor or Lamb nomogram were highly correlated (coefficient 0.994) and pair-wise comparison revealed no significant effect of the choice of nomogram ($P = 0.19$, Wilcoxon paired rank-sum).

The data from dichromatic animals form clusters close to the genetically predicted peaks. The histogram means are uniformly shifted to wavelengths 3–7 nm below the mean values reported by Tovée *et al.* (1992). This result, in common with the recent analysis of marmoset cone pigments by Kawamura *et al.* (2001), suggests that the peak sensitivity of marmoset pigments may be at slightly shorter wavelengths than originally reported by Tovée *et al.* However, as can be seen in Fig. 3A, the normalized error curves have broad minima, which limits the precision with which the peak wavelength can be specified. For the population of cells tested, a shift of 3 nm on the wavelength scale produced a mean increase in normalized error of 1.62% ($n = 34$, s.d. = 5.5%). Furthermore, there was a small but consistent effect of stimulus spatial frequency on the spectral position of the best-fit nomogram: measurements made at low spatial frequency (< 0.05 cycles deg^{-1}) returned a best-fit wavelength which was, on average, 2.1 nm longer than that obtained at optimum spatial frequency. The basis of this effect is unclear. In summary, it is safe to conclude that the genetic analysis correctly predicts the ML cone pigment complement in marmosets. Although the physiological data suggest that the spectral peaks of the marmoset cone opsins may be at slightly shorter wavelengths than originally reported, this question cannot be answered definitively by the present study.

Temporal-chromatic properties of PC cells

The temporal-chromatic properties of 87 PC cells were measured. All cells had receptive fields within 15 deg retinal eccentricity; the majority of these (75/87, 86%) were within 5 deg of the centre of the fovea. Anatomical reconstruction confirmed the location of 66 (76%) of the cells in the PC layers. The anatomical position of the remaining cells was not verified but their encounter position within the recording track, their eye dominance, and their spatial response properties, were consistent with their identity as PC cells. The data set comprised

only cells in which the response amplitude exceeded 10 impulses s^{-1} for at least one stimulus condition. Data were obtained from nine genetically predicted dichromats, and six trichromats. Two of the trichromats showed the 556/563 genotype; four showed the 543/563 genotype. One further female animal was not genotyped, but was identified by the physiological analysis described below as a 543/563 trichromat. We refer to the 543/563 and 556/563 phenotypes as $\Delta 20$ nm and $\Delta 7$ nm, respectively, according to the spectral separation between the M and L cone pigments. Some data presented here originated from animals used in our previous studies, and was reanalysed for the current study (White *et al.* 1998; Solomon *et al.* 1999).

Figure 4A shows an example of PC cell responses as a function of relative phase (θ) of the red and green light-emitting diodes (LEDs). This animal showed the $\Delta 20$ nm genotype, and this cell shows the characteristic response signature of green-on and green-off PC cells (Smith *et al.* 1992; Yeh *et al.* 1995). The response minimum is close to in-phase diode modulation at low temporal frequencies, and the minimum is at a progressively more retarded green diode phase with increasing temporal frequency. The opposite pattern was shown by red-on and red-off PC cells,

in which response minima moved to a progressively more advanced green diode phase with increasing temporal frequency. The majority (25/31, 81%) of PC units in the $\Delta 20$ nm phenotype exhibited overt red–green opponent responses at low temporal frequencies; the remaining units were more responsive to luminance modulation at all temporal frequencies. These data are consistent with the examples shown by Yeh *et al.* (1995) and support the idea that, in the same way as for macaque monkey (Smith *et al.* 1992; Lankheet *et al.* 1998), there is a temporal delay in the inhibitory opponent input to PC pathway cells in the marmoset.

Overt red–green opponent responses were not observed in PC cells in the $\Delta 7$ nm phenotype. Figure 4B shows typical responses of a PC cell, in one $\Delta 7$ nm animal (MY85). The response minimum is close to out-of-phase diode modulation at all temporal frequencies tested. Nevertheless, the following analysis showed that responses in both trichromatic phenotypes are consistent with at least partial segregation of M and L cones to receptive field centre and surround mechanisms.

We fitted data with the linear vector model developed and described fully by Smith *et al.* (1992). The response vector (amplitude and phase) of each cone type is predicted

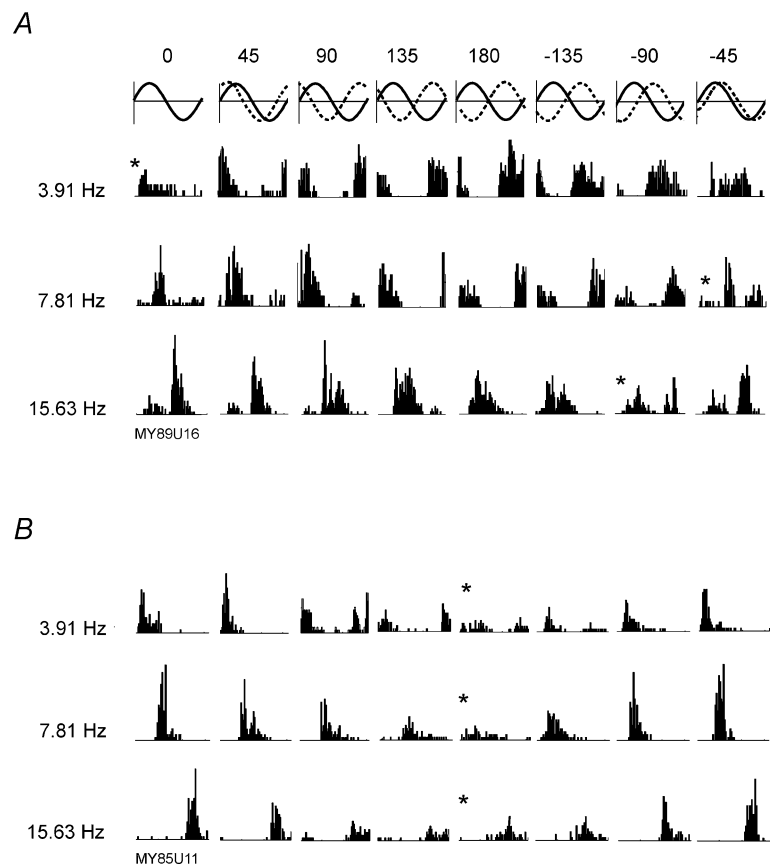


Figure 4. Responses of PC cells in two trichromatic phenotypes to one cycle of modulation at different relative diode phases.

About 8 s of activity are averaged in each histogram. A shows responses of one cell in the $\Delta 20$ nm phenotype; responses in the $\Delta 7$ nm phenotype are shown in B. The temporal waveform of the stimulus is depicted above the histograms. Continuous line, red LED; dashed line, green LED. Asterisks mark the histograms with minimum amplitude.

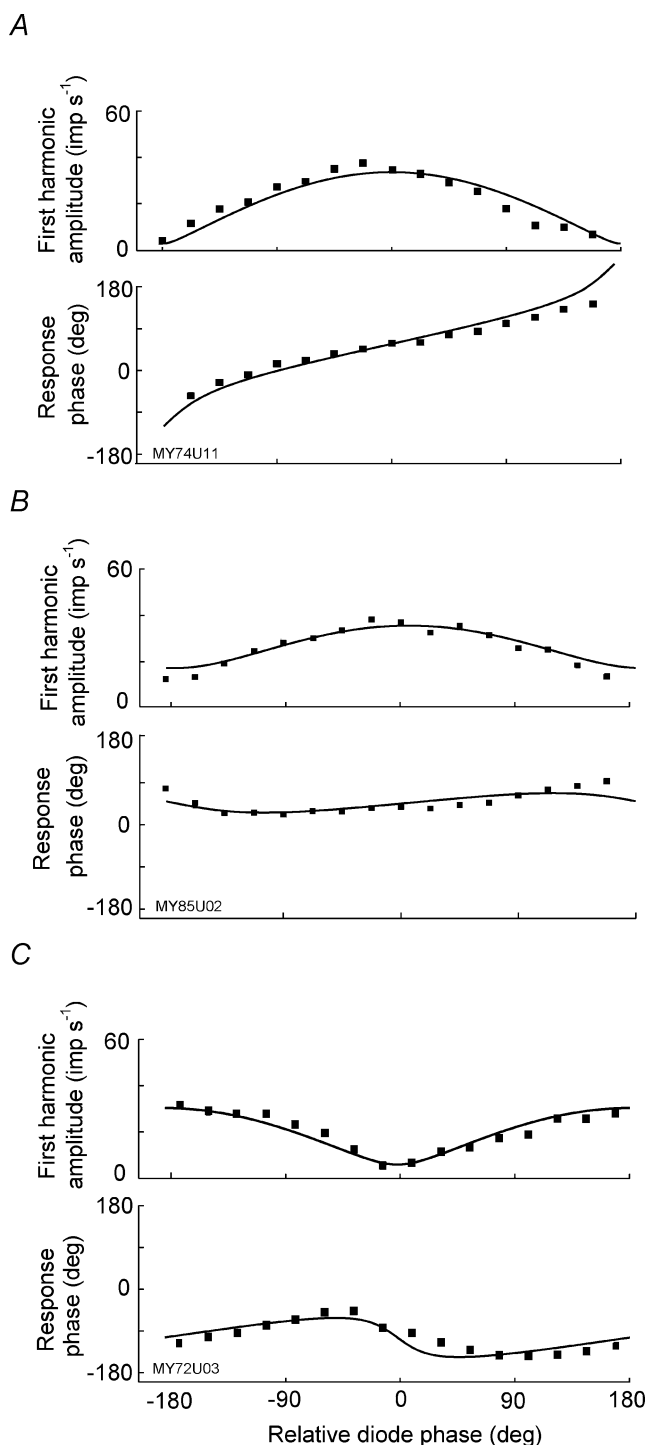


Figure 5. Comparison of PC cell response amplitude and phase as a function of relative diode phase in different colour vision phenotypes

One cell in the 556 nm phenotype is shown in A. Cells in the $\Delta 7$ nm and $\Delta 20$ nm phenotypes are shown in B and C, respectively. Continuous lines show predictions of the model described in the text. Note the minimum response amplitude for in-phase diode modulation in the $\Delta 20$ nm phenotype.

by vector addition of the response to the red and green LEDs, as a function of green LED phase. For the 543 nm (M) cone, the response vector (\vec{M}) is:

$$\vec{M} = \vec{R}_M + \vec{G}_M i \theta \quad (1)$$

where \vec{R}_M is the amplitude and phase of response to the red LED, \vec{G}_M is the amplitude and phase of response to the green LED, θ is the phase of the green LED and i is the imaginary unit $\sqrt{-1}$. Parallel calculations are made for the other cone types. Expressed as Michelson contrast, out-of-phase modulation of the LEDs gives 23% contrast in the 543 cone, 8% contrast in the 556 cone, and 26% contrast in the 563 cone. The 543 cone response is dominated by the green LED; responses of the 556 and 563 (L) cones are dominated by the red LED.

The response of a cone-opponent cell, \vec{C} , is predicted from a weighted sum of the cone response vectors. For a cell receiving excitatory input from M cones, the predicted response is:

$$\vec{C} = A(W\vec{M}i\theta_M + (1 - W)\vec{L}i\theta_\Delta) \quad (2)$$

where \vec{C} is cell phase and amplitude, A is an amplitude scaling factor, W is the M cone weight, \vec{M} and \vec{L} are the response vectors from eqn (1), θ_M is the phase of the M cone and θ_Δ is the phase difference between the M and L cones (Smith *et al.* 1992). Cell responses were fitted to this model by least-squares minimization, with free parameters A , W , θ_M and θ_Δ . The M/L cone balance parameter (W) was constrained to lie between 0 and 1. Other parameters were unconstrained. Data were fitted to the model as described above for the CIE set. In order to avoid convergence to local minima in the error function, parameters were given initial values within the range of feasible solutions (see also Smith *et al.* 1992; Yeh *et al.* 1995).

Cell responses were predicted using nomograms at the spectral positions (543 nm, 556 nm, 563 nm) predicted by the genetic analysis. Example responses and model outputs for modulation at 3.9 Hz are shown in Fig. 5. The model provides a good fit to the data for the trichromatic phenotypes. For modulation at 3.9 Hz, the root mean error (RME) for amplitude was 4.1 impulses s^{-1} for the $\Delta 7$ nm phenotype (s.d. = 2.3, $n = 28$) and 5.1 impulses s^{-1} for the $\Delta 20$ nm phenotype (s.d. = 2.9, $n = 31$). The RME for phase was 2.4 deg for the $\Delta 7$ nm phenotype (s.d. = 1.1, $n = 28$) and 2.2 deg for the $\Delta 20$ nm phenotype (s.d. = 0.8, $n = 31$). Fits made using 'wrong' cone fundamentals (i.e. other than predicted by the genetic analysis) normally returned higher residual errors, or did not converge on a feasible solution. For the $\Delta 7$ nm phenotype we repeated the predictions using a non-opponent ('in-phase') combination of the cone

mechanisms. Under this condition the RME for amplitude was unchanged ($4.1 \text{ impulses s}^{-1}$ (s.d. = 2.3, $n = 28$) but the phase RME increased to 6.3 deg (s.d. = 6.8, $n = 28$). As previously reported for the $\Delta 20 \text{ nm}$ phenotype (Yeh *et al.* 1995) we found for both trichromatic phenotypes that the L cone (563 nm) weight was normally greater in 'red-on' and 'red-off' cells ($\Delta 20 \text{ nm}$ phenotype, mean 0.44, s.d. = 0.33, $n = 17$; $\Delta 7 \text{ nm}$ phenotype, mean 0.66, s.d. = 0.09, $n = 15$) than in 'green-on' and 'green-off' cells ($\Delta 20 \text{ nm}$ phenotype, mean 0.33, s.d. = 0.11, $n = 14$; $\Delta 7 \text{ nm}$ phenotype, mean 0.46, s.d. = 0.18, $n = 13$).

For a small number of cells ($n = 5$) in each phenotype the responses to temporal frequencies between 2 and 16 Hz were measured in order to characterize the phase delay between excitatory and inhibitory cone mechanisms (θ_{Δ}). Figure 6 shows mean values for five cells in the $\Delta 20 \text{ nm}$ phenotype (Fig. 6A) and five cells in the $\Delta 7 \text{ nm}$ phenotype (Fig. 6B). The phase delay increases in a linear way with temporal frequency, consistent with fixed latency between opponent mechanisms in both the $\Delta 20 \text{ nm}$ and $\Delta 7 \text{ nm}$ phenotypes. Results from other cells (where a smaller range of temporal frequencies was tested) were consistent with this pattern. For all cells, the phase delay, expressed as latency difference, was 3–11 ms. These values are within the range reported for macaque and marmoset (Smith *et al.* 1992; Yeh *et al.* 1995; Benardete & Kaplan, 1997; Kilavik *et al.* 2003). These data show that red–green opponent responses in both trichromatic phenotypes could arise from centre–surround interactions.

Contrast sensitivity of PC cells

We next measured responses to luminance and chromatic modulation at different stimulus contrasts. The reasoning behind this experiment was as follows. The spectral sensitivity peaks of M and L cones are less widely separated in trichromatic marmosets than in routine trichromats such as macaque monkey. If the PC pathway were specifically adapted to serve the red–green dimension

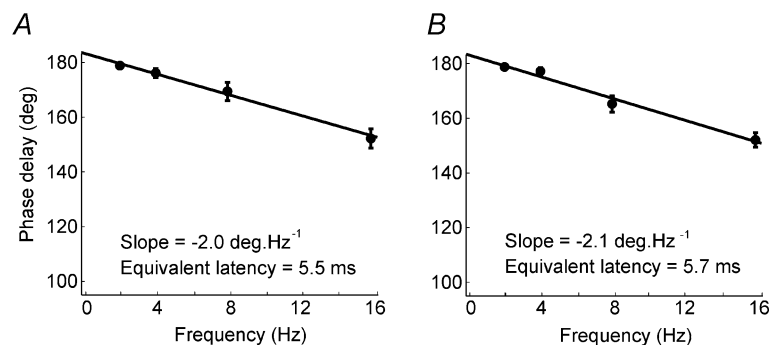
of colour vision, then it might be expected that some plastic neuronal mechanism would act to compensate for the reduced ML difference signal, prior to transmission as trains of action potentials in ganglion cell axons. Reports of chromatic selectivity in ganglion cell receptive fields (Martin *et al.* 2001; Reid & Shapley, 2002) give *a priori* evidence for such a possibility. Alternatively, if opponent responses are a simple by-product of centre–surround interactions, then the amplitude in response to chromatic modulation should be determined by the separation between M and L pigments. Our data are consistent with the latter hypothesis, as follows.

Example contrast-response functions for the 556 nm dichromat, $\Delta 7 \text{ nm}$ trichromatic, and $\Delta 20 \text{ nm}$ trichromatic phenotypes are shown in Fig. 7A–C. Responses of the majority of PC cells were well-fitted by linear regression of response amplitude on stimulus contrast for both luminance and chromatic modulation conditions (Derrington *et al.* 1984; Derrington & Lennie, 1984; Smith *et al.* 1992; Yeh *et al.* 1995; Solomon *et al.* 1999). The regression y -intercept was constrained to zero. We previously showed that addition of a 'spontaneous activity' (positive y -axis intercept) or 'contrast threshold' (positive x -axis intercept) term to contrast–response curves in marmoset LGN does not significantly reduce the average residual error for fits of this kind (Solomon *et al.* 1999). Cells showing marked response saturation for luminance modulation ($n = 4$) at contrasts above 30% were excluded from the analysis.

Group data for all cells tested in the three phenotypes are shown in Fig. 7D–F. There is a progressive reduction in the mean chromatic response gain from the $\Delta 20 \text{ nm}$ phenotype (mean = $0.30 \text{ impulses s}^{-1} \%^{-1}$, s.d. = 0.17, $n = 25$), to the $\Delta 7 \text{ nm}$ phenotype (mean = $0.09 \text{ impulses s}^{-1} \%^{-1}$, s.d. = 0.07, $n = 28$) and finally to the dichromatic phenotypes (mean = $0.05 \text{ impulses s}^{-1} \%^{-1}$, s.d. = 0.05, $n = 24$). These differences are significant at the 5% probability level (Wilcoxon rank-sum test). We conclude

Figure 6. Estimation of centre–surround phase delay

Mean and s.e.m. of the centre–surround phase delay parameter θ_{Δ} for 5 cells in the $\Delta 20 \text{ nm}$ trichromat phenotype are shown in A, and for 5 cells in the $\Delta 7 \text{ nm}$ trichromat phenotype are shown in B. Equivalent response latency was estimated from the slope of the least-square regression lines (continuous lines).



that under uniform stimulus conditions, the chromatic responsivity in PC cells is primarily determined by the spectral separation of M and L cones.

Receptive field dimensions of PC cells

We next asked whether the spatial properties of PC receptive fields show systematic variation between dichromatic and trichromatic animals. Responses to high-contrast achromatic drifting gratings were analysed using the difference-of-Gaussians (DOG) function as described in the Methods section. Figure 8 shows examples of spatial tuning functions for PC cells in a 543/563 trichromat (Fig. 8A) and a 563 dichromat (Fig. 8B). The achromatic spatial frequency tuning curves show band pass characteristic, and response amplitude is comparable for the two cells. Red–green and luminance modulation

sensitivity for the same cells is shown in Fig. 8C and D. The luminance modulation sensitivity is comparable for the two cells, but responses to red–green modulation are only evident in the cell from the trichromatic animal.

Figure 9A shows PC centre radius as a function of receptive field eccentricity for the three genotypes studied. Most points fall within the range given in previous studies of marmoset PC cells (Kremers & Weiss, 1997; White *et al.* 2001; Kilavik *et al.* 2003). In the present study, where three different phenotypes are distinguished, it can be seen that the data sets show almost complete overlap. We conclude that the generation of ML opponent signals does not compromise the spatial resolving properties of the PC cell system for high-contrast stimuli. The mean receptive field centre radius for foveal (= 3 deg eccentricity) receptive fields in dichromats (0.039 deg, s.d. = 0.01, $n = 29$) was

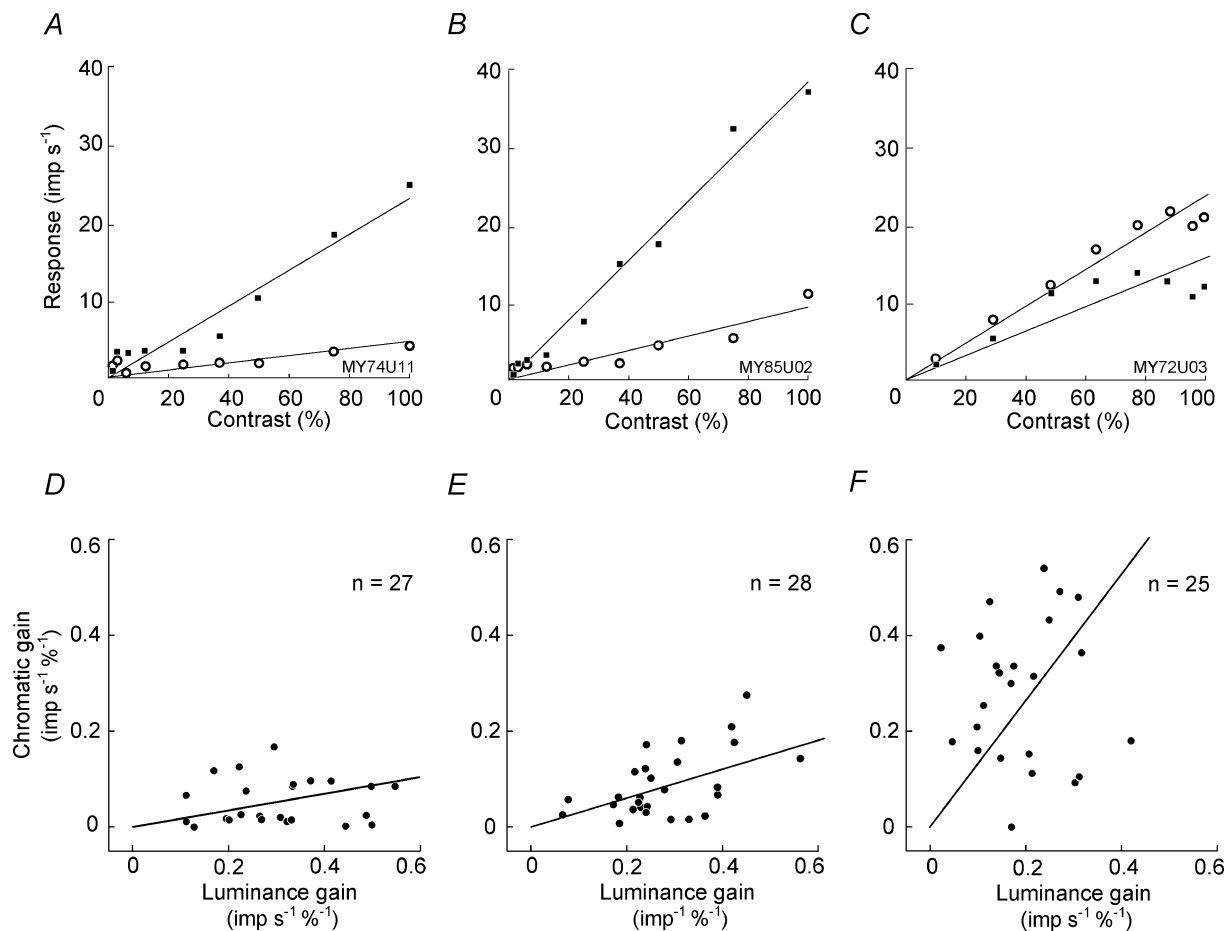


Figure 7. Contrast sensitivity

The top panels show example contrast–response functions for PC cells in three phenotypes. A, 556 nm dichromat; B, $\Delta 7$ nm trichromat; C, $\Delta 20$ nm trichromat. ●, luminance modulation; ○, red–green chromatic modulation. The lower panels show response gain for the two stimulus conditions for PC cells in these phenotypes. D, 556 nm dichromat; E, $\Delta 7$ nm trichromat; F, $\Delta 20$ nm trichromat.

close to that in $\Delta 20$ nm trichromats (mean = 0.041 deg, s.d. = 0.02, $n = 21$, $P = 0.99$, Wilcoxon rank-sum test). However, the mean centre radius for extrafoveal (> 3 deg eccentricity) receptive fields in $\Delta 20$ nm trichromats (mean = 0.095 deg, s.d. 0.061, $n = 22$) was slightly larger than in dichromats (0.072 deg, s.d. 0.039, $n = 18$, $P < 0.01$, Wilcoxon rank-sum test). This difference is addressed further in the Discussion section.

Regression analysis showed no relation between centre diameter and chromatic contrast sensitivity in the $\Delta 20$ nm phenotype ($r^2 = 0.05$, $n = 14$). Kilavik *et al.* (2003) reported relatively large centre sizes among a sample of PC cells in one trichromatic marmoset. However, these authors could not exclude the possibility that sub-optimal optics had led to spuriously large centre size

measurements in this animal. In our hands, cells showing vigorous red–green opponent responses included some of the smallest fields we measured. We did encounter one cell in the PC layers of a $\Delta 20$ nm phenotype animal that showed a large centre size ($r_c = 0.74$ deg) and vigorous response to high contrast red–green modulation. However, the following observations suggest that this cell may have been an ‘ectopic’ MC or KC cell. First, the cell showed strong temporal band-pass tuning, consistent with phasic response properties. Second, the cell showed very high sensitivity to luminance modulation and saturating response at high ($> 25\%$) luminance contrast. Third, the response to luminance modulation exceeded (at least double) the response to red–green modulation at all contrast levels tested. We conclude that the response to red–green modulation in this cell can be attributed to high

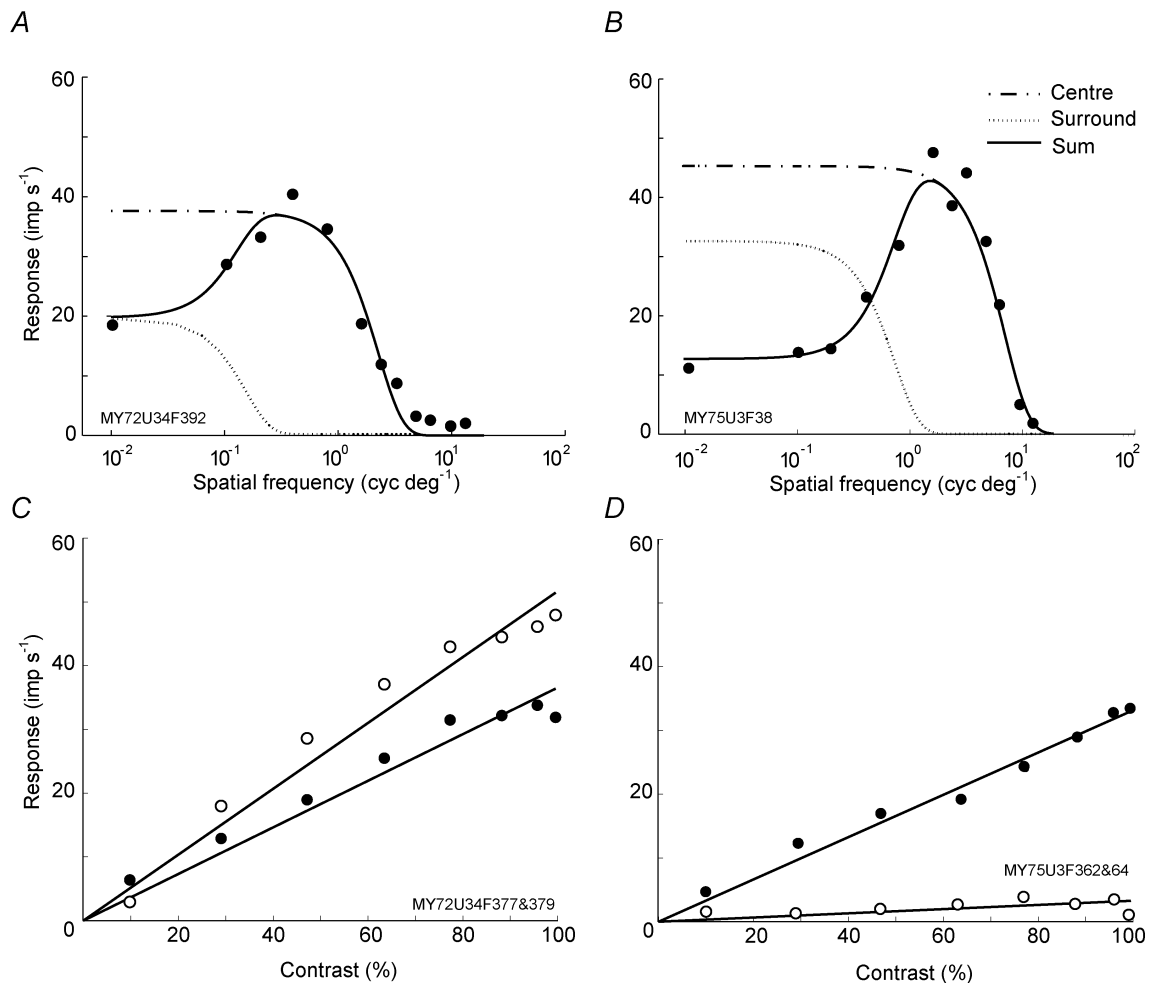


Figure 8. Spatial and chromatic properties of PC cells

Upper panels show spatial frequency tuning curves for achromatic sine gratings. Lower panels show contrast–response functions as in Fig. 9. Responses of a PC cell in the $\Delta 20$ nm trichromatic phenotype are shown in A and C. Responses in a 563 nm dichromat are shown in B and D. Lines in A and B show difference-of-Gaussians fit and components. Lines in C and D show linear fits as in Fig. 9. ● in C and D, luminance modulation; ○ in C and D, red–green chromatic modulation.

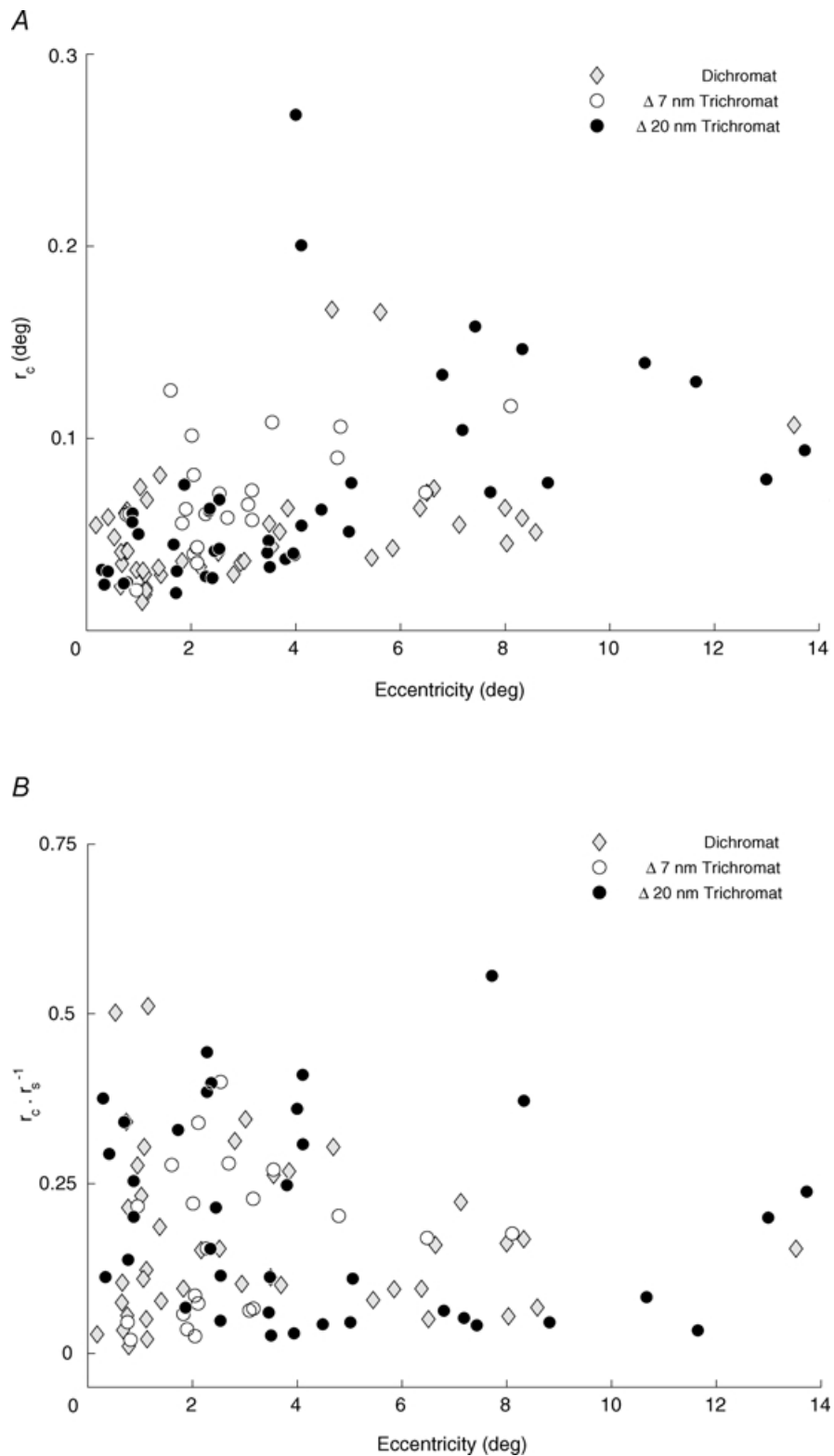


Figure 9. Comparison of receptive field dimensions in different colour vision phenotypes

Stimuli were achromatic sine gratings. Each point in *A* shows centre radius (r_c) from the difference-of-Gaussians model described in the text. The ratio of centre radius to surround radius (r_s) is shown in *B*.

luminance sensitivity rather than opponent interactions. This cell was therefore excluded from the statistical analysis of achromatic contrast sensitivity given below.

Wiesel & Hubel (1966) distinguished a subclass of PC cells ('Type II') which showed spatial overlap between centre and surround receptive field mechanisms. This and subsequent studies in macaque and marmoset showed that the majority of Type II cells receive input from S cones, whereas most cells receiving input from M and L cones show centre-surround receptive field spatial structure (Derrington & Lennie, 1984; Crook *et al.* 1988; Croner & Kaplan, 1995; Kremers & Weiss, 1997; Lee *et al.* 1998; Kilavik *et al.* 2003). We asked whether the relative size of centre and surround in PC cells is different in dichromatic and trichromatic marmosets. The result (Fig. 9B) is consistent with that obtained in marmoset by Kremers & Weiss (1997) and Kilavik *et al.* (2003), with the exception that we did not see differences in the average centre size between dichromatic and trichromatic marmosets, as reported by the latter authors. In the present study the mean centre:surround ratios were: dichromat, 0.162, s.d. 0.123, $n = 42$; $\Delta 20$ nm trichromat, 0.197, s.d. 0.148, $n = 37$; $\Delta 7$ nm trichromat, 0.162, s.d. 0.110, $n = 22$. These values are consistent with data from macaque (Derrington & Lennie, 1984; Croner & Kaplan, 1995). Pairwise comparison of the three groups showed no differences in the relative radius of centre and surround mechanisms ($P > 0.25$, Wilcoxon rank-sum test). In summary, these data confirm that centre-surround spatial antagonism is a feature of PC cells in dichromatic and trichromatic primates, with the surround radius normally three to 10 times greater than the centre radius.

Achromatic contrast sensitivity of PC cells

Finally, we examined the relationship between receptive field centre radius and achromatic contrast sensitivity (Fig. 10). Previous studies in the mammalian subcortical visual system demonstrated that within each functional cell class, large receptive fields have lower contrast sensitivity (per unit area) than small receptive fields (reviewed by Troy & Shou, 2002). Thus, within each class, the integrated sensitivity ('volume') of the receptive field centre is approximately constant throughout the retina. For primates it has been demonstrated that the volume of MC centres is, on average, greater than that of PC centres (Irvin *et al.* 1993; Croner & Kaplan, 1995; White *et al.* 2001). However, a systematic comparison of dichromatic and trichromatic PC cells has not previously been made.

In each panel of Fig. 10, sensitivity is plotted as a function of radius on a dual logarithmic scale. Linear regression fits to the data for receptive field centres show an approximately inverse relationship of peak sensitivity to area. Most points fall close to a line with slope close to -2 , as predicted for the inverse area-sensitivity relationship. There is substantial overlap between data sets for centre mechanisms. Regression analysis of the log-transformed data gives a small but significant ($P < 0.01$) difference in achromatic sensitivity of the centre mechanism when

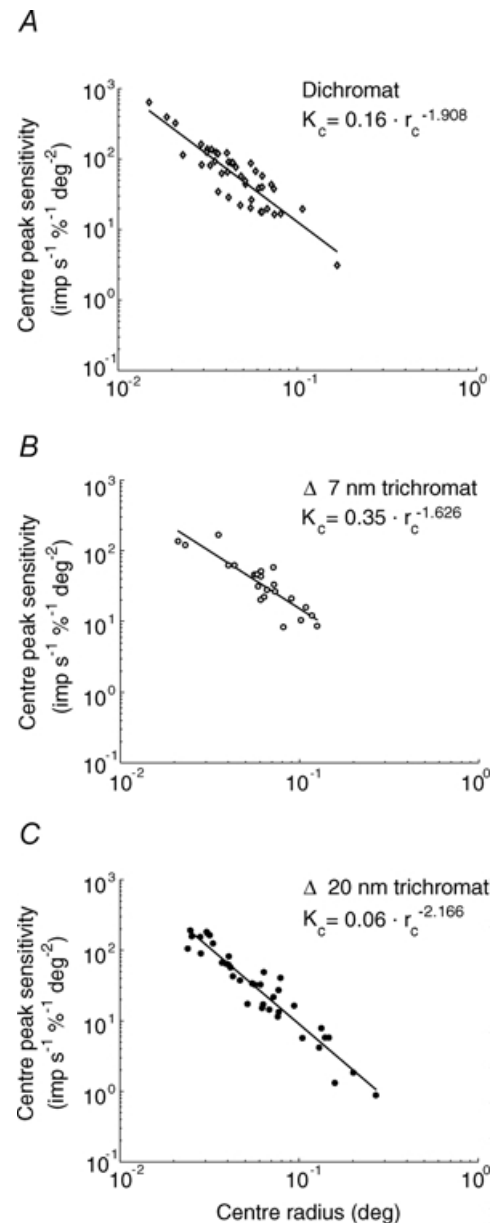


Figure 10. Achromatic contrast sensitivity and centre radius in different colour vision phenotypes

Stimuli were achromatic sine gratings. Continuous lines show linear regression on log-transformed data for the centre components. Abbreviations: K_c , centre sensitivity; r_c , centre radius.

dichromat and $\Delta 20$ nm trichromat data are compared. At a centre radius of 0.04 deg (the mean value for foveal cells) the separation between the regression lines corresponds to 21.5% greater achromatic sensitivity in the dichromatic than in the $\Delta 20$ nm phenotype. The data from the $\Delta 7$ nm phenotype were not subjected to regression analysis because only a small number of foveal receptive fields were measured in this phenotype (see Fig. 9). In summary, these data suggest that expression of colour opponent responses is associated with a modest decrease in achromatic contrast sensitivity of the receptive field centre component.

Discussion

Origin of red–green opponent responses

In all trichromatic primates studied so far, the amplitude and phase of red–green opponent responses in PC cells shows marked dependence on the temporal frequency of stimulation (Gouras & Zrenner, 1979; Smith *et al.* 1992; Yeh *et al.* 1995; Lankheet *et al.* 1998; Lee *et al.* 2000). Although there is disagreement about the details, it is generally agreed that the retinal wiring which produces centre–surround antagonism could account for the temporal-frequency dependence of chromatic responsivity. This idea is based on data obtained from the visual system of the cat, which showed that the surround mechanism of ‘X-brisk-sustained’ cells lags the centre mechanism by 3–10 ms (Frishman *et al.* 1987; Troy & Shou, 2002). Our data show that the same range of delay values (3–11 ms) can account for the range of temporal-chromatic behaviour of PC cells in animals with M and L pigments separated by 20 or 7 nm. Furthermore, we find great consistency in the centre–surround spatial structure of PC cells in dichromatic and trichromatic phenotypes. These data are consistent with other studies where either spatial or chromatic properties of PC-pathway cells in macaque, capuchin monkey and howler monkey have been measured (Hicks *et al.* 1983; Lee *et al.* 1990; Smith *et al.* 1992; Lee *et al.* 2000; Saito *et al.* 2004). Together with the current study these findings give circumstantial evidence that the chromatic properties of PC cells are governed by the spatial properties, and not *vice versa*.

Relation of PC pathway responses to chromatic discrimination

In the two trichromatic phenotypes which we studied, the sensitivity to red–green chromatic modulation increased

with increasing spectral separation of the cone pigments. By contrast, the red–green colour discrimination capacity of human anomalous trichromats does not show strong linear dependence on the separation of M and L cone spectra (reviewed by MacLeod, 2003). For example, Shevell *et al.* (1998) report close to normal chromatic discrimination capacity in human anomalous trichromats with M and L pigments separated by only 6 nm. Likewise, behavioural tests on a close relative of the marmoset, the saddle-backed tamarin *Saguinus fuscicollis*, showed near-normal red–green discrimination in a trichromatic female with M and L pigments separated by less than 15 nm (Jacobs *et al.* 1987). Our results suggest that the reduced range of inputs available from narrowly separated photoreceptor spectra is not compensated by increases in neuronal gain prior to the geniculo-cortical synapse. This conclusion is, however, limited by the fact that we did not make systematic measurements of signal-to-noise ratio in the present study.

The PC pathway in colour and spatial vision

Our findings are consistent with the hypothesis that the parvocellular-projecting midget ganglion cell class carries signals underlying the red–green dimension of colour vision (Shapley & Perry, 1986; Mollon, 1989; Wässle & Boycott, 1991). Firstly, the majority (greater than 80%) of foveal PC cells in the $\Delta 20$ nm trichromat showed red–green opponent responses, and very small receptive fields, as expected for input from a small number of cones. This is consistent with the connectivity of the midget bipolar-ganglion cell system in the fovea (Wässle & Boycott, 1991; Chan *et al.* 2001). Secondly, the receptive field size of PC cells was the same in dichromatic and trichromatic animals (Figs 9 and 10).

We did not see evidence for a distinct subpopulation of large, spatially non-opponent (‘Type II’, Wiesel & Hubel, 1966) red–green opponent receptive fields in the PC layers in this study, or in the koniocellular layers in a previous study (White *et al.* 1998). However, we cannot rule out the possibility that such a distinct population exists, as they have only been encountered as a very low proportion of PC cells (Wiesel & Hubel, 1966; Dreher *et al.* 1976). Our analysis of spatial properties did, however, show that as for macaque PC cells (Derrington & Lennie, 1984), there is a wide range of centre–surround size ratios, not only among trichromatic marmosets, but also among dichromats. This is consistent with the suggestion by Derrington *et al.* (1984) that Wiesel & Hubel’s (1966) Type I and Type II categories of red–green opponent PC cells are the extremes of a continuum rather than two distinct functional classes.

Although only a small number of cells with extrafoveal receptive fields were recorded, the range of receptive field sizes is also consistent with input from the midget ganglion cell pathway (Goodchild *et al.* 1996). The following observations suggest there is some chromatic selectivity in the PC pathway in the peripheral retina. Firstly, we saw no correlation between centre radius and red–green sensitivity across the range of eccentricities measured (0–13 deg). However, the convergence of cones to PC cells increases substantially over this range of eccentricities. It follows that PC receptive field centres should draw from multiple cones, and thus receive spectrally mixed input if the draw is indiscriminant, at eccentricities above 8 deg. For example, at 8–10 degrees, the local cone density is close to 650 cones deg⁻² (Troilo *et al.* 1993; Wilder *et al.* 1996). A receptive field with a centre radius of 0.15 deg (see Fig. 9A) would encompass the area of 46 cones, and the morphology of midget bipolar and midget ganglion cells at 10 deg is consistent with convergence of at least 20 cones to midget ganglion cells (Chan *et al.* 2001). The consistency between these estimates is improved by considering that the point-spread function would produce a modest (< 5 min radius at half-height, see, e.g. Navarro & Artal, 1993) enlargement of the receptive field centre. Secondly, the average receptive field radius of extra-foveal cells in the Δ20 nm trichromatic phenotype was slightly larger than that in dichromats, as would be expected if the receptive field were expanded to make chromatic specific connections. This suggests that, as shown for PC ganglion cells in macaque (De Monasterio & Gouras, 1975; Martin *et al.* 2001; Reid & Shapley, 2002) the PC pathway in peripheral marmoset retina shows some selectivity for chromatically specific connections. Recordings targeted to the peripheral visual field are required to resolve this question conclusively.

References

- Baylor DA, Nunn BJ & Schnapf JL (1987). Spectral sensitivity of cones of the monkey *Macaca fascicularis*. *J Physiol* **390**, 145–160.
- Benardete EA & Kaplan E (1997). The receptive field of the primate P retinal ganglion cell, I: Linear dynamics. *Visual Neurosci* **14**, 169–186.
- Brainard DH (1996). Cone contrast and opponent modulation color spaces. In *Human Color Vision*, ed. Kaiser PK & Boynton GM, pp. 563–577. Optical Society of America, Washington, DC.
- Cavonius CR & Estévez O (1975). Sensitivity of human colour mechanisms to gratings and flicker. *J Opt Soc Am A* **65**, 966–968.
- Chan TL, Martin PR, Clunas N & Grünert U (2001). Bipolar cell diversity in the primate retina: Morphologic and immunocytochemical analysis of a New World monkey, the marmoset *Callithrix jacchus*. *J Comp Neurol* **437**, 219–239.
- Croner LJ & Kaplan E (1995). Receptive fields of P and M ganglion cells across the primate retina. *Vision Res* **35**, 7–24.
- Crook JM, Lange-Malecki B, Lee BB & Valberg A (1988). Visual resolution of macaque retinal ganglion cells. *J Physiol* **396**, 205–224.
- De Monasterio FM & Gouras P (1975). Functional properties of ganglion cells of the rhesus monkey retina. *J Physiol* **251**, 167–195.
- De Monasterio FM, Gouras P & Tolhurst DJ (1975). Concealed colour opponency in ganglion cells of the Rhesus monkey retina. *J Physiol* **251**, 217–229.
- De Valois RL, Abramov I & Jacobs GH (1966). Analysis of response patterns of LGN cells. *J Opt Soc Am* **56**, 966–977.
- Derrington AM, Krauskopf J & Lennie P (1984). Chromatic mechanisms in lateral geniculate nucleus of macaque. *J Physiol* **357**, 241–265.
- Derrington AM & Lennie P (1984). Spatial and temporal contrast sensitivities of neurones in lateral geniculate nucleus of macaque. *J Physiol* **357**, 219–240.
- Dreher B, Fukada Y & Rodieck RW (1976). Identification, classification and anatomical segregation of cells with X-like and Y-like properties in the lateral geniculate nucleus of Old-World primates. *J Physiol* **258**, 433–452.
- Frishman LJ, Freeman AW, Troy JB, Schweitzer-Tong DE & Enroth-Cugell C (1987). Spatiotemporal frequency responses of cat retinal ganglion cells. *J General Physiol* **89**, 599–628.
- Goodchild AK, Ghosh KK & Martin PR (1996). Comparison of photoreceptor spatial density and ganglion cell morphology in the retina of human, macaque monkey, cat, and the marmoset *Callithrix jacchus*. *J Comp Neurol* **366**, 55–75.
- Gouras P & Zrenner E (1979). Enhancement of luminance flicker by color-opponent mechanisms. *Science* **205**, 587–589.
- Hicks TP, Lee BB & Vidyasagar TR (1983). The responses of cells in macaque lateral geniculate nucleus to sinusoidal gratings. *J Physiol* **337**, 183–200.
- Hunt DM, Williams AJ, Bowmaker JK & Mollon JD (1993). Structure and evolution of the polymorphic photopigment gene of the marmoset. *Vision Res* **33**, 147–154.
- Ingling CR & Martinez E (1985). The spatio-temporal properties of the r-g cell channel. *Vision Res* **18**, 379–390.
- Irvin GE, Casagrande VA & Norton TT (1993). Center/surround relationships of magnocellular, parvocellular, and koniocellular relay cells in primate lateral geniculate nucleus. *Visual Neurosci* **10**, 363–373.
- Jacobs GH (1996). Primate photopigments and primate color vision. *Proc Natl Acad Sci U S A* **93**, 577–581.
- Jacobs GH, Neitz J & Crognale M (1987). Color vision polymorphism and its photopigment basis in a callitrichid monkey. (*Saguinus Fuscicollis*) *Vision Res* **27**, 2089–2100.

- Kawamura S, Hirai M, Takenaka O, Radlwimmer FB & Yokoyama S (2001). Genomic and spectral analyses of long to middle wavelength-sensitive visual pigments of common marmoset. (*Callithrix jacchus*). *Gene* **269**, 45–51.
- Kilavik BE, Silveira LC & Kremers J (2003). Centre and surround responses of marmoset lateral geniculate neurones at different temporal frequencies. *J Physiol* **546**, 903–919.
- Kremers J & Weiss S (1997). Receptive field dimensions of lateral geniculate cells in the common marmoset (*Callithrix jacchus*). *Vision Res* **37**, 2171–2181.
- Kremers J, Weiss S & Zrenner E (1997). Temporal properties of marmoset lateral geniculate cells. *Vision Res* **37**, 2649–2660.
- Lamb TD (1995). Photoreceptor spectral sensitivities: common shape in the long-wavelength region. *Vision Res* **35**, 3083–3091.
- Lankheet MJM, Lennie P & Krauskopf J (1998). Temporal–chromatic interactions in LGN P-cells. *Visual Neurosci* **15**, 47–54.
- Lee BB, Kremers J & Yeh T (1998). Receptive fields of primate retinal ganglion cells studied with a novel technique. *Visual Neurosci* **15**, 161–175.
- Lee BB, Pokorny J, Smith VC, Martin PR & Valberg A (1990). Luminance and chromatic modulation sensitivity of macaque ganglion cells and human observers. *J Opt Soc Am A* **7**, 2223–2236.
- Lee BB, Silveira LCL, Yamada ES, Hunt DM, Kremers J, Martin PR, Troy JB & da Silva M (2000). Visual responses of ganglion cells of a New-World primate, the capuchin monkey, *Cebus apella*. *J Physiol* **528**, 573–590.
- Lee BB, Valberg A, Tigwell DA & Tryti J (1987). An account of responses of spectrally opponent neurons in macaque lateral geniculate nucleus to successive contrast. *Proc R Soc Lond Series B Biol Sci* **230**, 293–314.
- Lee BB, Wehrhahn C, Westheimer G & Kremers J (1993). Macaque ganglion cell responses to stimuli that elicit hyperacuity in man: detection of small displacements. *J Neurosci* **13**, 1001–1009.
- Lennie P, Haake PW & Williams DR (1991). The design of chromatically opponent receptive fields. In *Computational Models of Visual Processing*, ed. Movshon JA, pp. 71–82. MIT Press, Cambridge, MA, USA.
- MacLeod DIA (2003). The Verreist Lecture. Colour discrimination, colour constancy and natural scene statistics. In *Normal and Defective Colour Vision*, ed. Mollon JD, Pokorny J & Knoblauch K, pp. 189–217. Oxford University Press, Oxford.
- Martin PR, Lee BB, White AJR, Solomon SG & Rüttiger L (2001). Chromatic sensitivity of ganglion cells in the peripheral primate retina. *Nature* **410**, 933–936.
- Mollon JD (1989). “Tho’ she kneel’d in that place where they grew. . .” (The uses and origins of primate color vision). *J Exp Biol* **146**, 21–38.
- Mollon JD, Bowmaker JK & Jacobs GH (1984). Variations of colour vision in a New World primate can be explained by polymorphism of retinal photopigments. *Proc R Soc Lond Series B Biol Sci* **222**, 373–399.
- Mollon JD & Jordan G (1988). Eine evolutionäre Interpretation des menschlichen Farbensehens. *Die Farbe* **35**, 139–170.
- Navarro R & Artal P (1993). Modulation transfer of the human eye as a function of retinal eccentricity. *J Opt Soc Am A* **10**, 201–212.
- Paulus W & Kröger-Paulus A (1983). A new concept of retinal colour coding. *Vision Res* **23**, 529–540.
- Reid RC & Shapley RM (2002). Space and time maps of cone photoreceptor signals in macaque lateral geniculate nucleus. *J Neurosci* **22**, 6158–6175.
- Rodieck RW (1991). Which cells code for color? *From Pigments to Perception: Advances in Understanding Visual Processes*, ed. Lee BB, pp. 83–93. Plenum Press, London.
- Rushton WAH, Spitzer Powell D & White KD (1973). Exchange thresholds in dichromats. *Vision Res* **13**, 992–1002.
- Saito CA, da Silva Filho M, Lee BB, Bowmaker JK, Kremers J & Silveira LCL (2004). *Alouatta* trichromatic color vision – single-unit recording from retinal ganglion cells and microspectrophotometry. *ARVO Abstracts Invest Ophthalmol Visual Sci*, Program No. 4276.
- Shapley R & Perry VH (1986). Cat and monkey retinal ganglion cells and their visual functional roles. *Trends Neurosci* **9**, 229–235.
- Shevell SK, He JC, Kaintz P, Neitz J & Neitz M (1998). Relating color discrimination to photopigment genes in deutan observers. *Vision Res* **38**, 3371–3376.
- Smith VC, Lee BB, Pokorny J, Martin PR & Valberg A (1992). Responses of macaque ganglion cells to the relative phase of heterochromatically modulated lights. *J Physiol* **458**, 191–221.
- Solomon SG, White AJR & Martin PR (1999). Temporal contrast sensitivity in the lateral geniculate nucleus of a New World monkey, the marmoset *Callithrix jacchus*. *J Physiol* **517**, 907–917.
- Solomon SG, White AJR & Martin PR (2002). Extraclassical receptive field properties of parvocellular, magnocellular and koniocellular cells in the primate lateral geniculate nucleus. *J Neurosci* **22**, 338–349.
- Tovée MJ, Bowmaker JK & Mollon JD (1992). The relationship between cone pigments and behavioural sensitivity in a New World monkey (*Callithrix jacchus jacchus*). *Vision Res* **32**, 867–878.
- Travis DS, Bowmaker JK & Mollon JD (1988). Polymorphism of visual pigments in a callitrichid monkey. *Vision Res* **28**, 481–490.
- Troilo D, Howland HC & Judge SJ (1993). Visual optics and retinal cone topography in the common marmoset (*Callithrix jacchus jacchus*). *Vision Res* **33**, 1301–1310.

- Troy JB & Shou T (2002). The receptive fields of cat retinal ganglion cells in physiological and pathological states: where we are after half a century of research. *Prog Ret Eye Res* **21**, 263–302.
- Wässle H & Boycott BB (1991). Functional architecture of the mammalian retina. *Physiol Rev* **71**, 447–480.
- Weiss S, Kremers J & Maurer J (1998). Interaction between rod and cone signals in responses of lateral geniculate neurons in dichromatic marmosets (*Callithrix jacchus*). *Visual Neurosci* **15**, 931–943.
- White AJR, Goodchild AK, Wilder HD, Sefton AE & Martin PR (1998). Segregation of receptive field properties in the lateral geniculate nucleus of a New-World monkey, the marmoset *Callithrix jacchus*. *J Neurophysiol* **80**, 2063–2076.
- White AJR, Solomon SG & Martin PR (2001). Spatial properties of koniocellular cells in the lateral geniculate nucleus of the marmoset *Callithrix jacchus*. *J Physiol* **533**, 519–535.
- Wiesel TN & Hubel DH (1966). Spatial and chromatic interactions in the lateral geniculate body of the rhesus monkey. *J Neurophysiol* **29**, 1115–1156.
- Wilder HD, Grünert U, Lee BB & Martin PR (1996). Topography of ganglion cells and photoreceptors in the retina of a New World monkey: the marmoset *Callithrix jacchus*. *Visual Neurosci* **13**, 335–352.
- Yeh T, Lee BB, Kremers J, Cowing JA, Hunt DM, Martin PR & Troy JB (1995). Visual responses in the lateral geniculate nucleus of dichromatic and trichromatic marmosets (*Callithrix jacchus jacchus*). *J Neurosci* **15**, 7892–7904.

Acknowledgements

We are grateful to Ana Lara and Dean Matin for technical assistance, to J. Forte and W. J. Dobbie for assistance with data collection, to A. J. Benjafield from University of Sydney and Joy Parker from Monash University Animal Services for assistance with the genetic analysis. B. Dreher and U. Grünert provided helpful comments on the manuscript. The work was supported by Australian NHMRC grant 253621, Australian Research Council grant A00104053, an Australian Postgraduate Award to E.B., and a University of Sydney Medical Faculty Postgraduate Research Scholarship to S.S.

Author's present address

S. G. Solomon: University Laboratory of Physiology, University of Oxford, Parks Road, Oxford OX1 3PT, UK